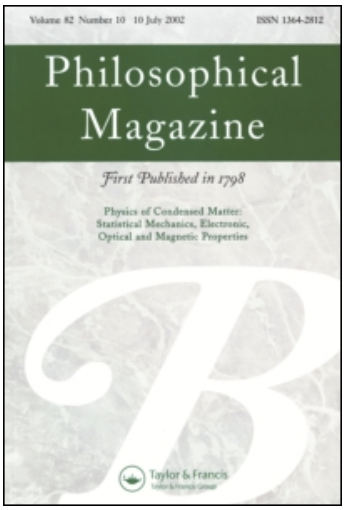

Philosophical Magazine Part B
Publication details, including instructions for authors and subscription information:
http://www.informaworld.com/smpp/title~content=t713836176

Director textures of the Nèel inversion wall in a liquid crystal polymer

Ding-Kuo Dingt [a]; Bih-yaw Jin [b]; Janelle Gunther [c]; Edwin L. Thomas [d]
[a] TECO Electric and Machinery Co., Ltd, Taipei, Taiwan [b] International Center for Material Research, Kawasaki, Kanagawa, Japan [c] Department of Chemistry, National Taiwan University, Taipei, Taiwan [d] Department of Materials Science and Engineering, Massachusetts Institute of Technology, Cambridge, Massachusetts, USA

Online Publication Date: 01 December 1997

To cite this Article Dingt, Ding-Kuo, Jin, Bih-yaw, Gunther, Janelle and Thomas, Edwin L.(1997)'Director textures of the Nèel inversion wall in a liquid crystal polymer',Philosophical Magazine Part B,76:6,951 — 960
To link to this Article: DOI: 10.1080/01418639708243141
URL: http://dx.doi.org/10.1080/01418639708243141

PHILOSOPHICAL MAGAZINE B, 1997, VOL. 76, NO. 6, 951–960

Director textures of the Néel inversion wall in a liquid crystal polymer

By DING-KUO DING†‡, BIH-YAW JIN§, JANELLE GUNTHER‖ and EDWIN L. THOMAS‖

† TECO Electric and Machinery Co., Ltd, Taipei, Taiwan 102
‡ International Center for Material Research, Kawasaki, Kanagawa 213 Japan
§ Department of Chemistry, National Taiwan University, Taipei, Taiwan 106
‖ Department of Materials Science and Engineering, Massachusetts Institute of Technology, Cambridge, Massachusetts 02139, USA

[*Received 6 January 1997 and accepted in revised form 25 April 1997*]

ABSTRACT

A solution of the director orientation function is presented for Néel inversion walls created in a liquid crystal by application of a magnetic field. The theoretical model is used to simulate director trajectories across walls as a function of both the elastic anisotropy and the orientation of the wall with respect to the applied field. The gradual transition of the defect structures from Néel bend walls to Néel splay walls as the angle between the wall and the magnetic field is varied is also presented. Micrographs obtained via atomic force microscopy on a thermotropic liquid crystalline polymer are used to test and evaluate the theoretical model. Visualization of director textures using the lamellar decoration technique shows the theoretical and experimental results to be in good agreement. The results were used to determine that the sample had an elastic anisotropy of approximately 0·5, implying that $k_{11} = 3k_{33}$.

§1. INTRODUCTION

Liquid crystals are characterized by a non-polar vector called the director **n** which indicates the locally preferred orientation of the molecules. When a nematic liquid crystal of positive diamagnetic anisotropy is placed in a magnetic field, the director tends to orient along the field direction. Regions of uniform orientation along the field direction can be separated by an inversion wall. Upon crossing the wall, the director orientation changes by an angle of π. There are three principal types of wall. The first are pure twist walls, which are analogous to Bloch walls in magnetic-spin systems (Kléman 1983). The other two types of director wall are analogous to Néel bend and Néel splay walls. The director field distribution across these two dimensional non-singular wall defects were first studied by Helfrich (1968).

Although optical microscopy has been used to study inversion walls, there are many difficulties and ambiguities associated with this technique (Donald 1985). Another technique, known as lamellar decoration, permits high-resolution imaging of the director field via transmission electron microscopy (Thomas and Wood 1985), scanning electron microscopy or atomic force microscopy (AFM). The latter method offers many advantages for detailed imaging of director textures such as ease of sample preparation and non-destructiveness, enabling successive imaging of evolutionary variations in the director field. Much important information on inversion

walls can be obtained via AFM, including the characteristic coherence length and the elastic anisotropy of the liquid crystal polymer (Ding and Thomas 1993).

In the present work, the lamellar decoration technique has been used in conjunction with AFM to study the director orientation distribution near Néel bend and splay walls. This subject has not been previously examined in detail because of the difficulty in handling the nonlinear partial differential equation that describes the director orientation. A gradual transition of wall structure from splay to bend as a function of the orientation of the wall and the applied field is discussed in detail in terms of both experimental and theoretical results.

§2. Mathematical treatment

The conventional free-energy density for a nematic in a magnetic field consists of a linear gradient elastic term and a nonlinear magnetic term given as

$$g = \tfrac{1}{2}[k_{11}(\nabla\cdot\mathbf{n})^2 + k_{22}(\mathbf{n}\cdot\nabla\times\mathbf{n})^2 + k_{33}(\mathbf{n}\times\nabla\times\mathbf{n})^2 - \tfrac{1}{2}\chi_a(\mathbf{n}\cdot\mathbf{H})^2], \tag{1}$$

where k_{11}, k_{22} and k_{33} are the splay, twist and bend elastic constants respectively H is the magnetic field and χ_a is the magnetic susceptibility anisotropy (deGennes 1974). The two terms in the free energy balance each other. The linear elastic term tends to disperse distortions, while the nonlinear magnetic term globally reorients the director and localizes the distortions. The latter is the mechanism responsible for the formation of inversion walls. Equation (1) can be simplified for thin films, where the director is confined to lie in the plane. In this situation, no twist is allowed. The only degree of freedom then becomes ϕ, which is the angle between the director and a fixed axis contained in the plane. If a strong magnetic field is applied parallel to the plane of a thin film with the director confined to the x–y plane, then the free-energy density can then be rewritten as

$$g = \tfrac{1}{2}\left[(k_{11}\sin^2\phi + k_{33}\cos^2\phi\left(\frac{\partial\phi}{\partial x}\right)^2 + (k_{11}\cos^2\phi + k_{33}\sin^2\phi)\left(\frac{\partial\phi}{\partial y}\right)^2 + 2(k_{33}-k_{11})\sin\phi\cos\phi\left(\frac{\partial\phi}{\partial x}\right)\left(\frac{\partial\phi}{\partial y}\right)\right] - \tfrac{1}{2}\chi_a H^2\cos^2(\phi-\phi_H), \tag{2}$$

where ϕ_H is determined by the direction of the magnetic field.

The total free energy of this system can be written as

$$G = \int_{-\infty}^{+\infty}\int_{-\infty}^{+\infty} g\,\mathrm{d}x\,\mathrm{d}y. \tag{3}$$

The Euler–Lagrange equation that minimizes the total free energy is then

$$0 = (k_{11}\sin^2\phi + k_{33}\cos^2\phi)\left(\frac{\partial^2\phi}{\partial x^2}\right) + (k_{11}\cos^2\phi + k_{33}\sin^2\phi)\left(\frac{\partial^2\phi}{\partial y^2}\right) + (k_{11}-k_{33})\sin\phi\cos\phi\left[\left(\frac{\partial\phi}{\partial x}\right)^2 - \left(\frac{\partial\phi}{\partial y}\right)^2\right] + (k_{33}-k_{11})\sin(2\phi)\left(\frac{\partial^2\phi}{\partial x\,\partial y}\right) + \chi_a H^2\cos(\phi-\phi_H)\sin(\phi-\phi_H). \tag{4}$$

The total energy remains constant when the coordinates are rotated. Thus the director field of the inversion wall is only a function of a single variable, say y. Consider the case where an inversion wall is formed at an angle with respect to the applied field. The new axis parallel to the inversion wall is chosen so that the director field is given by $n = (\cos[\phi(y)], \sin[\phi(y)])$ and the magnetic field by $H = (\cos \phi_H, \sin \phi_H)$. The Euler–Lagrange equation then reduces to

$$0 = (k_{11} \cos^2 \phi + k_{33} \sin^2 \phi)\frac{d^2\phi}{dy^2} + (k_{33} - k_{11}) \sin \phi \cos \phi \left(\frac{d\phi}{dy}\right)^2 + \chi H^2 \cos(\phi - \phi_H) \sin(\phi - \phi_H). \tag{5}$$

This equation can be solved by multiplying by $\frac{1}{2}(d\phi/dy)$ and integrating. This yields

$$(k_{11} \cos^2 \phi + k_{33} \sin^2 \phi)\left(\frac{d\phi}{dy}\right)^2 = \chi_a H^2 \sin^2(\phi - \phi_H), \tag{6}$$

where the integration constant vanishes because $d\phi/dy$ approaches zero as ϕ approaches ϕ_H. The elastic anisotropy $\epsilon = (k_{11} - k_{33})/(k_{11} + k_{33})$ is now introduced together with a new characteristic length $\zeta = (1/H)[(k_{11} = k_{33})/\chi_a]^{1/2}$. A dimensionless distance $u = y/\zeta$ can be defined in order to rewrite above equation as

$$[1 + \epsilon \cos(2\phi)]\left(\frac{d\phi}{du}\right)^2 = \sin^2(\phi - \phi_H). \tag{7}$$

The quantity $d\phi/du$ is obtained by taking the square root of the previous equation:

$$\frac{d\phi}{du} = \frac{|\sin(\phi - \phi_H)|}{[1 + \epsilon \cos(2\phi)]^{1/2}}. \tag{8}$$

This equation can now be integrated to obtain u as a function of ϕ:

$$u(\phi) = \int_{-(\pi/2)+\phi_H}^{\phi} \frac{[1 + \epsilon \cos(2\phi)]^{1/2}}{|\sin(\phi - \phi_H)|} d\phi \qquad \text{for } u \geqslant 0,$$

$$u(\phi) = -\int_{\phi}^{-(\pi/2)+\phi_H} \frac{[1 + \epsilon \cos(2\phi)]^{1/2}}{|\sin(\phi - \phi_H)|} d\phi \qquad \text{for } u < 0. \tag{9}$$

The limits of integration were carefully chosen in order to satisfy the boundary conditions and to avoid singularities. For the simplest case where elastic constants are equal, the Euler–Lagrange equation reduces to

$$\left(\frac{d\phi}{du}\right)^2 = \sin^2(\phi - \phi_H), \tag{10}$$

where $u = y/\zeta$, and ζ is the characteristic length equal to $(1/H)(k/2\chi_a)^{1/2}$. Here ζ takes the same value as the traditional magnetic coherence length ξ defined by deGennes. The analytic solution for the director field in the equiconstant case (Helfich 1968) can now be written as

$$\phi = \phi_H - 2 \arctan\left[\exp\left(-\frac{y}{\zeta}\right)\right], \tag{11}$$

where the value of ϕ is equal to $-\pi/2 + \phi_H$ if y is equal to zero, and the value ϕ approaches $-\pi + \phi_H$ or ϕ_H when u approaches negative or positive infinity respectively.

§3. Experimental procedure

A main-chain thermotropic nematic liquid crystalline polyether, 1-(4-[hydroxy-4′-biphenyl)-2-(4-hydroxyphenyl)propane with 1,5-dibromopentane) (TPP5), of $\bar{M}_n = 11{\cdot}2\,\mathrm{kg\,mol^{-1}}$ and $\bar{M}_w/\bar{M}_n = 2{\cdot}5$ was used for this study. A 1–2 μm thin film in the nematic state was sheared on a glass slide using a razor blade. To create the inversion walls, the specimen was first aligned in a 13·5 T magnetic field which was oriented in the plane of the sample and perpendicular to the shearing direction. The annealing process was conducted at 160°C for 30 min. The sample was then quenched to room temperature at a rate of $10^{\circ}\mathrm{C\,s^{-1}}$ using a flow of nitrogen gas. In the final processing step, the lamellar decoration technique (Thomas and Wood 1985) was used to cause the sample to partially crystallize into a lamellar morphology. The variations in director field distribution are made visible by AFM of the lamellae which protrude above the film surface by 2–4 nm and are normal to the local director. A Digital Instruments multimode atomic force microscope and Nanoscope III controller were used to acquire 8 μm by 8 μm height images of the liquid crystal. The atomic force microscope was operated in contact mode and was equipped with 200 μm SiN_3 cantilevers. Typical applied forces were a few millinewtons with scan rates of 5 Hz.

§4. Results and discussion

The general solution of the director orientation distribution across an inversion wall as a function of field direction for a nematic liquid crystal with elastic anisotropy requires the solution of a two-dimensional nonlinear partial differential equation (eqn. (5)). Rotation of the coordinate system shows that the problem is actually one dimensional and therefore much easier to solve (our eqn. (9)). When the coordinate system is rotated so that the x axis is along the inversion wall, the y axis now becomes the only degree of freedom.

Simulations for the director orientation across a Néel wall for the equiconstant case ($k_{11} = k_{33}$) as a function of the orientation of the wall with respect to the field direction are shown in fig. 1. The proportions of bend and splay character in the wall depend on the wall orientation. The first plot (fig. 1 (*a*)) shows the case where the wall and the magnetic field are parallel. In this situation the Néel wall has pure bend character. The last plot (fig. 1 (*e*)) shows a splay wall that results when the wall and the magnetic field are orthogonal. The results for intermediate angles (figs. 1 (*b*)–(*d*)) show how the Néel wall makes a gradual change from bend to splay character. It is evident that a Néel wall formed at 45° to the field (fig. 1 (*c*)) embodies an equal mixture of both bend and splay. Note that the director orientation of the Néel bend wall ($\phi_H = 0°$) is precisely orthogonal to that of the Néel splay wall ($\phi_H = 90°$).

The AFM image in fig. 2 shows the Néel wall used for the analysis in this paper. The angle ϕ_H between the wall and the applied field varies gradually as the wall is followed from the lower right to the upper left side of the micrograph. Note that, as ϕ_H varies, so does the amount of splay and bend character in that region of the wall. Based on the work of Ding and Thomas (1993) the polymer TPP5 has $\epsilon = +0{\cdot}5$ and $k_{11} = 3k_{33}$; so it would prefer bend distortions over splay (the polymer MEBB5 described in that publication was renamed TPP5). Since the lamellae

Fig. 1

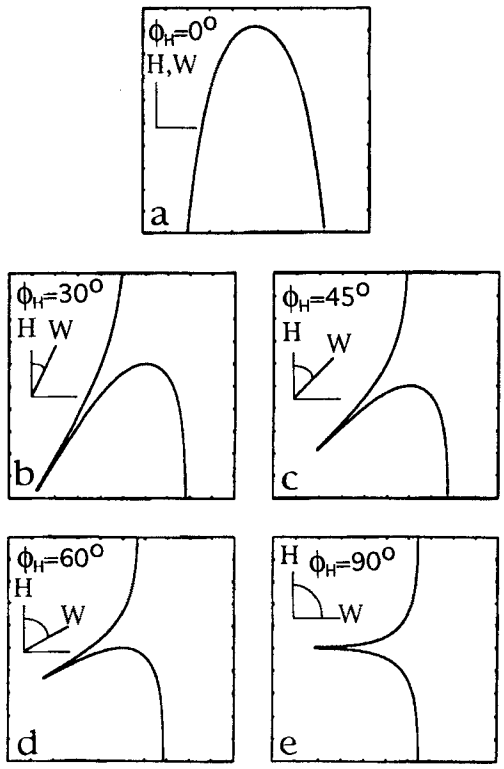

A series of plots showing the director trajectory across a wall as a function of ϕ_H, the angle between the wall W and the applied field H. In all cases $\epsilon = 0$ (equiconstant case).

grow perpendicular to the director, what appears in the AFM image as a splay wall is in fact a bend wall for the reasons discussed earlier. To determine the director field using the AFM image, we first produce a hand tracing of lines normal to the lamellae. The result is a rough map of the director field which is shown in fig. 3 (*a*). The region of the wall towards the lower right of the image (i.e. $\phi_H = -13°$) has both splay and bend character. Then, as the wall gradually curves and becomes nearly parallel to the field (i.e. the region with $\phi_H = 13°$), the director exhibits much more bend character. In the actual AFM image this is seen as increasing amounts of splay in the lamellae.

In order to obtain a quantitative comparison between data and theory, several criteria were selected. First, the wall (or segments thereof) should be isolated from other walls or defects that might introduce additional distortions in the director field. Secondly, the wall should have a relatively constant ϕ_H. This is an important criterion because a curved wall in fact represents a superposition of many director field solutions of various ϕ_H, a situation which is more difficult to model mathematically. On the basis of these criteria, the relatively straight portion of the wall at $\phi_H = 53°$ was selected for the analysis.

To produce a more reliable map of the director field than that from fig. 3 (*a*), the NIH-Image software package was used to extract the x–y location of the lamellae

Fig. 2

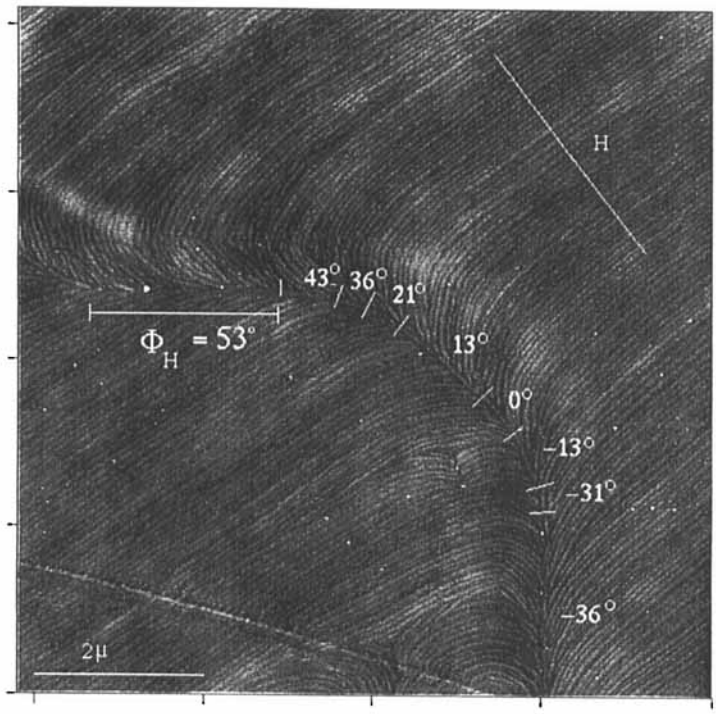

An AFM image depicting the Néel wall analysed in this paper. The numerical labels indicate the value (in degrees) of ϕ_H, which is the angle between the wall and the applied field. The lines drawn normal to the centreline of the wall separate segments of differing ϕ_H. The straight segment with $\phi_H = 53°$ was used for the mathematical analysis of the director field distribution.

(fig. 3(*b*)). These coordinates were then entered into a Matlab script that reconstructed the lamellar trajectories and then calculated and plotted line segments orthogonal to them (fig. 3(*c*)). These line segments represent the local orientation of the director field with respect to the lamellae. These segments were then used to reconstruct a more accurate tracing of the entire director field (fig. 3(*d*)) than would have been obtained by complete free hand drawing.

Simulations of the director trajectory as a function of ϕ_H and elastic anisotropy ϵ were made using a Matlab script file. Equation (9) was solved numerically with cubic splines used to skip the singular points. Some examples of the results are shown in figs. 4(*a*) and (*b*). The former shows several plots which have the same value of elastic anisotropy ($\epsilon = 0{\cdot}5$) but varying values of ϕ_H. It can be seen that small differences in ϕ_H do not produce large changes in the directory trajectory. For example, there is not a great difference between the results for 50, 53 and 55°. However, there are significant differences between the results for 53° and either 40 or 60°. A similar situation exists for variations in elastic anisotropy at fixed ϕ_H (see fig. 4((*b*)). The differences between simulations for *epsilon* = 0·4, 0·5 and 0·6 are almost undetectable. However, large changes in ϵ from $\epsilon = -1$ (easy splay) to $\epsilon = +1$ (easy bend) produce significant changes in the simulations.

Fig. 3

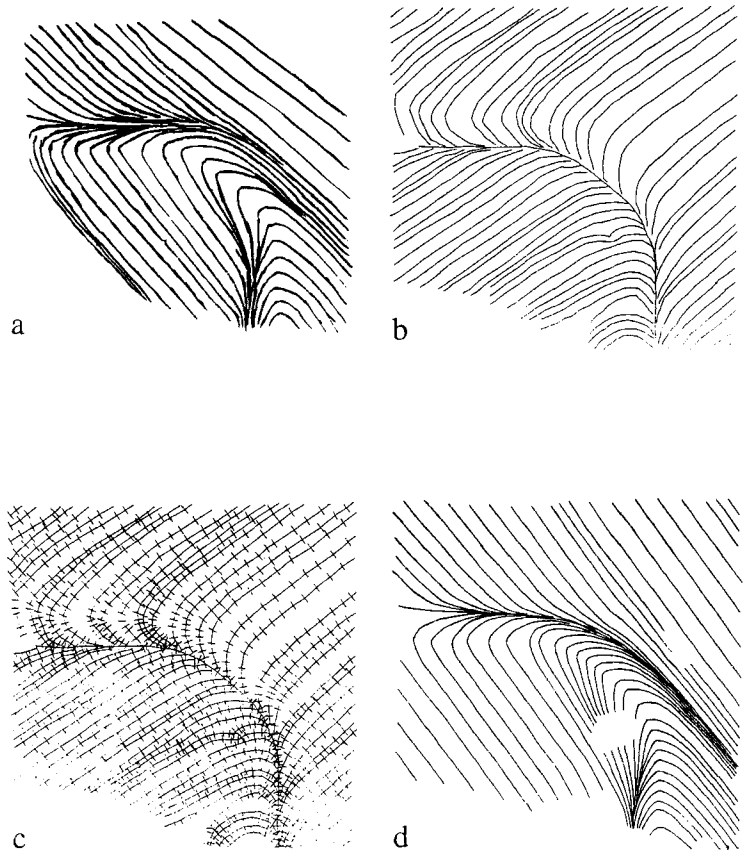

(*a*) A rough map of the director field distribution produced by hand tracing lines normal to the lamellae in the atomic force micrograph of fig. 2. (*b*) A plot of the lamellar trajectories generated from the atomic force micrograph shown in fig. 2. The NIH-Image software package was used to extract the coordinates of the lamellae. The results were then input to Matlab which produced the actual plot (*c*). This plot shows the orthogonal line segments generated by Matlab for the purpose of producing a partial map of the director field distribution. A Matlab script file was used to generate the line segments. These segments represent the local director orientation in regions where the director intersects a lamellar trajectory. (*d*) This plot depicts the final map of the director field distribution. The lines corresponding to the director orientation were produced by a small amount of hand tracing along the computer generated line segments from (*c*).

We now compare theory with experiment to illustrate the difference between good and bad fits of representative director fields. NIH Image was used to extract the coordinates of both the simulations and the director field distribution. The result was input to a Matlab script file that fits a polynomial to each set of coordinates. The curve obtained from Matlab was placed on the director field map so that the data and simulations would coincide at locations far from the center of the wall. The equations obtained from these operations were then used to obtain a rms error value in y for a fixed range in x, defined as $\langle R^2 \rangle^{1/2} = [\sum (y_{\text{data}} - y_{\text{theory}})^2]^{1/2}$. All curves

Fig. 4

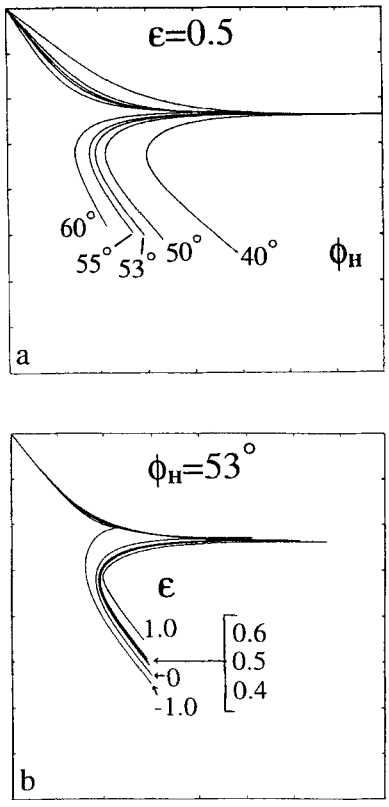

(*a*) A series of plots showing variations in the director distribution across walls for various values of ϕ_H with ϵ fixed at 0·5. Large changes in ϕ_H produce noticeable changes in the director trajectory. Changes of only a few degrees have a lesser effect. (*b*) A series of plots showing variations in the director distribution across walls for various values of ϵ for ϕ_H fixed at 53°. Small changes in ϵ are difficult to distinguish as indicated by the plots for $\epsilon = 0{\cdot}4$, 0·5 and 0·6. Large changes in ϵ (compare $\epsilon = 1{\cdot}0$ and $-1{\cdot}0$) show a marked difference, however. The former (1·0) clearly shows a higher degree of bend distortion while the latter shows more splay distortion.

were compared over the same range in x and with a comparable number of sampling points spread out uniformly along the contour.

The simulation in fig. 5(*a*) shows a 'bad fit' for $\epsilon = 0{\cdot}5$ and $\phi_H = 40°$. The corresponding rms error was 2·96. This high value resulted from the mismatch that occurred close to the centreline of the wall. At locations far from the wall, where the data and simulations are in good agreement, the rms error is much lower. In these particular regions, the rms is typically on the order of 0·15. Another example of a poor fit is shown in fig. 5(*b*). In this case, $\epsilon = -1{\cdot}0$ and $\phi_H = 53°$. Far from the wall, the rms error is again around 0·15, while over the entire contour it increases to a value of 0·72. Figure 5(*c*) shows an example of a 'best fit', defined as the simulation that produces the lowest rms error. As can be seen in this plot, there is very little deviation between the simulation and the data. As a

Fig. 5

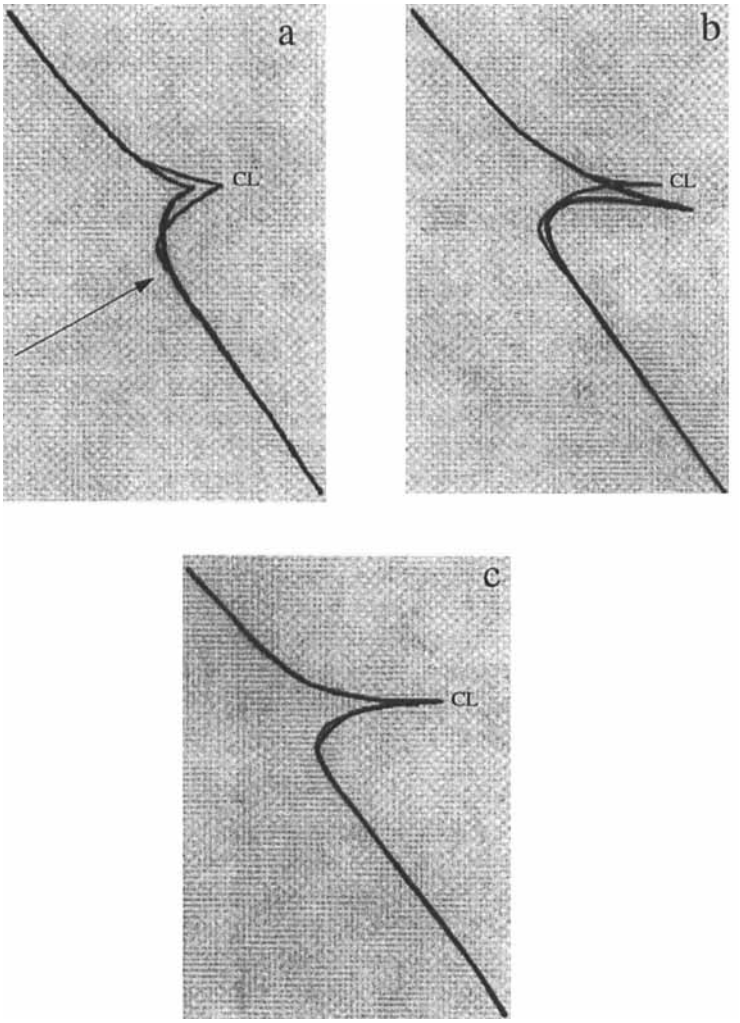

(*a*) An example of a 'bad fit' between the AFM image and simulations. The thick line represents a simulation for $\epsilon = -1{\cdot}0$ and $\phi_H = 53°$. The thin line (the cusp of the thin line is labelled CL) represents the data (taken from fig. 3 (*d*)). Far from the wall, the simulation and data do not differ appreciably. However as the centreline (labelled CL) of the wall is approached, the simulation begins to deviate markedly from the data. This first occurs in the location indicated by the arrow. For this particular simulation the overall rms error was 0·72. (*b*) An additional example of a 'bad fit' between data and experiment. In this case, $\phi_H = 40°$ and $\epsilon = 0{\cdot}5$. The thick and thin lines represent the simulation and data respectively. The mismatch is again most evident in the regions close to the centreline of the wall. The large mismatch in ϕ_H produced a more noticeable visual difference than did the mismatch in ϵ seen in (*a*). This is also supported by the larger value of the rms error in this simulation which was 2·96. (*c*) An example of a 'best fit' between data and experiment. In this case, $\phi_H = 53°$ and $\epsilon = 0{\cdot}5$. The overall rms error, 0·21 in this case, was the lowest obtained from all the comparisons that were made. The small amount of deviation indicated by the arrow resulted in a rms error of 0·19. This is only slightly larger than the rms error corresponding to the fit at regions far from the wall where the distortions are very low.

result the rms error is only 0·19, which is only slightly greater than the values obtained far from the wall where the distortions in the director field are much lower. The results from this particular data set show that the elastic anisotropy is approximately 0·5, which corresponds to our earlier measurement of $k_{11} = 3k_{33}$ using TPP5. This indicates that bend distortions are more favourable for this particular polymer. As the comparisons between data and simulation show, sensitivity to elastic anisotropy and wall orientation ϕ_H is greatest close to the centreline of the wall.

§ 5. Summary

The nonlinear partial differential equation describing director orientation across Néel walls in a liquid crystal polymer was solved for the general case of elastic anisotropy and variable angle of the wall with respect to the applied field. A computer program was used to create director orientation simulations as a function of both elastic anisotropy and wall angle with respect to the applied field. Experimental measurements of the director distribution were obtained by AFM of a polyether liquid crystal polymer using the lamellar decoration technique.

The type of numerical analysis described in this paper works best for long portions of a wall that are at a fixed orientation to the applied field and that are also free from the influences of nearby walls and other defects. Good fits between theory and simulations are obtained when these criteria are met. Calculations of the rms error in y values for a fixed range in x were used to make quantitative comparisons between simulations and data. The best fit to the data was selected by a combination of visual inspection and ranking of mean square error values. The fit of a wall at 53° with an elastic anisotropy of approximately 0·5 (i.e. $k_{11} = 3k_{33}$) agrees with earlier determinations of the elastic anisotropy of TPP5.

Acknowledgements

We thank Professor V. Percec of Case Western Reserve University for the TPP5 sample and useful discussions. Financial support was received from US Air Force Office of Scientific Research (AFOSR) grant No. 91-0078 and grant No. F49620-94-1-0024, as well as an AFOSR Graduate Fellowship (J.G.).

References

DeGennes, P. G., 1974, *The Physics of Liquid Crystals* (Oxford: Clarendon).
Ding, D.-K., and Thomas, E. L., 1993, *Macromolecules*, **26**, 6531.
Donald, A. M., 1985, *Phil. Mag.* B, **52**, 925.
Helfrich, W., 1968, *Phys. Rev. Lett.*, **21**, 1518.
Kléman, M., 1983, *Points, Lines, and Walls* (Chichester, West Sussex: Wiley).
Thomas, E. L., and Wood, B. A., 1985, *Faraday Discuss. Chem. Soc.*, **79**, 229.